Equivalent Circuit Model of Grid-Forming Converters With Circular Current Limiter for Transient Stability Analysis

Fan, Bo; Wang, Xiongfei

Published in:
IEEE Transactions on Power Systems

DOI (link to publication from Publisher):
10.1109/TPWRS.2022.3173160

Publication date:
2022

Document Version
Accepted author manuscript, peer reviewed version

This article has been accepted for publication in IEEE Transactions on Power Systems. This is the author's version which has not been fully edited and content may change prior to final publication. Citation information: DOI 10.1109/TPWRS.2022.3173160

Equivalent Circuit Model of Grid-Forming Converters With Circular Current Limiter for Transient Stability Analysis

Bo Fan, *Member, IEEE*, and Xiongfei Wang, *Senior Member, IEEE*

***Abstract*—This letter develops an equivalent circuit model of a grid-forming (GFM) converter with a circular current limiter and analyzes its transient stability. It is revealed that the inner control loop can be simplified as a voltage source behind an equivalent resistor. Based on the developed model, theoretical analysis and experimental tests demonstrate that the transient stability of a $P-f$ droop-controlled GFM converter with the circular current limiter can be assured whenever there exist stable equilibrium points.**

***Index Terms*—Equivalent circuit model, circular current limiter, grid-forming converter, transient stability.**

I. Introduction

In recent years, grid-forming (GFM) converters are treated as an effective solution for power grids with high penetration of converter-interfaced generators. By directly regulating the voltage and frequency based on the output power, the GFM converters can provide the grid operators with enhanced system stability and resilience [1].

Since the GFM converters behave as voltage sources behind impedance, their output currents are highly dependent on the electrical network conditions [1]. Further, the semiconductor-based converter can only handle tens of percent of over-current [2]. Current limiting strategies are hence required to protect the converters against large disturbances. Without changing the operating mode of the GFM converter, two typical current limiting methods are usually applied. The first one modifies the voltage reference based on the virtual impedance [3]. The second one directly restricts the current reference by using the current limiters [4].

With these methods, the transient stability of GFM converters, i.e., their ability to maintain synchronism with the power grid [5], needs to be evaluated. This problem is recently investigated in [3], [4]. In these studies, the voltage control loop is ignored with the assumption of its limited impact on transient stability. However, such a hypothesis does not hold for the circular current limiters [6] since the angle of the saturated current reference is determined by the voltage control loop. Therefore, the previous transient stability results [3], [4] are not applicable for GFM converters with circular current limiters. Moreover, although numerical-simulation-based methods, such as the phase plane analysis [7], may be applied to analyze the transient stability of GFM converters, they lack the physical insights into the control loops.

This work was supported by the European Union's Horizon 2020 Research and Innovation Programme under the Marie Skłodowska-Curie Grant Agreement 101031512 (FRESLING). *(Corresponding author: Xiongfei Wang.)*

Bo Fan and Xiongfei Wang are with the Department of Energy (AAU Energy), Aalborg University, Aalborg 9220, Denmark (e-mail: bof@et.aau.dk; xwa@et.aau.dk).

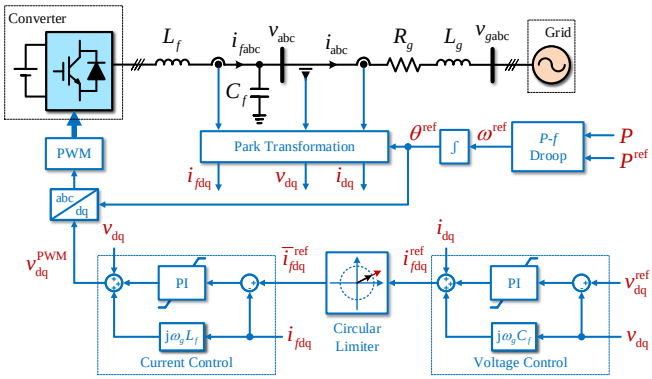

Fig. 1. Overall system diagram of a grid-connected GFM converter with the circular current limiter.

To this end, this letter attempts to investigate the physical insights into the circular current limiter with the following contributions:

1) An equivalent circuit model is established for the transient stability analysis of the GFM converter with a power-based synchronization mechanism. It is revealed that the inner control loop with the circular current limiter can be modeled as an equivalent resistor.

2) Based on the developed equivalent circuit model, the transient stability of $P-f$ droop control is analyzed. It is found that the GFM converter with the circular current limiter can synchronize with the power grid whenever there exist stable equilibrium points (SEPs).

Finally, these findings are validated by experimental tests.

II. Grid-Connected GFM Converter

Fig. 1 illustrates the system diagram of a GFM converter with the circular current limiter. The converter is connected to the grid through an LC-filter with L_f and C_f being its inductance and capacitance. L_g and R_g represent the grid impedance. The $P-f$ droop control is used to synchronize the converter with the grid. The voltage reference is achieved by the inner dual-loop proportional-integral (PI) control. The circular current limiter is implemented to protect the converter against over-current. v_{abc} and $v_{g\text{abc}}$ are the capacitor and grid voltages, respectively. i_{abc} and $i_{f\text{abc}}$ are the grid-side and converter-side currents, respectively. $(\cdot)_{\text{dq}}$ denotes a complex variable in the dq-frame.

The expression of the circular current limiter is given by

$$\bar{i}_{f\text{dq}}^{\text{ref}} = \sigma i_{f\text{dq}}^{\text{ref}}, \quad \sigma = \min\left\{1, I_M / \|i_{f\text{dq}}^{\text{ref}}\|\right\} \tag{1}$$

where $i_{f\text{dq}}^{\text{ref}}$ is the original current reference generated by the voltage control loop as shown in Fig. 1; $\bar{i}_{f\text{dq}}^{\text{ref}}$ is the saturated current reference; and I_M is the maximum allowable converter-side current magnitude. σ is a real-valued coefficient,

This article has been accepted for publication in IEEE Transactions on Power Systems. This is the author's version which has not been fully edited and content may change prior to final publication. Citation information: DOI 10.1109/TPWRS.2022.3173160

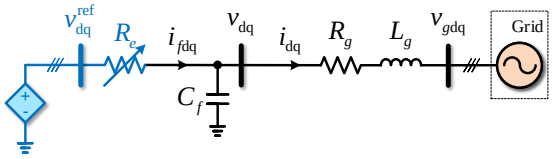

Fig. 2. Equivalent circuit of a grid-connected GFM converter. The blue part denotes the inner control loop with the circular current limiter.

i.e., only the magnitude i_{fdq}^{ref} is decreased when the circular current limiter is triggered, while its angle is kept unchanged.

The $P-f$ droop control is expressed as $\omega^{ref} = \omega_g + K_P(P^{ref} - P)$, where ω^{ref} is the angular frequency reference; ω_g is the grid angular frequency; K_P is the constant power control gain; P^{ref} is the active power reference; $P = 1.5\text{Re}\{v_{dq} i_{dq}^*\}$ is the active power output of the converter with $(\cdot)^*$ being the conjugate of a complex variable.

III. Proposed Equivalent Circuit Model

This section introduces an equivalent circuit model of the GFM converter shown in Fig. 1.

For the ease of the transient stability mechanism explanation of the GFM converter with the circular current limiter, the dynamics of the capacitor and inductor is ignored [2]–[4]. Since the inner control loop is usually designed to be much faster than the power one [1], [5], the current control loop dynamics is ignored for simplicity, i.e., $i_{fdq} = \bar{i}_{fdq}^{ref}$. Since the voltage integral controller is used to remove the steady-state impact of modeling errors [8], its dynamics can be ignored when the circular current limiter is not triggered [5], [9], i.e., $v_{dq} = v_{dq}^{ref}$ with v_{dq}^{ref} being the capacitor voltage reference. These assumptions are later justified by the experimental results presented in Section V.

When the circular current limiter is triggered, the voltage control loop is unable to regulate the capacitor voltage to its reference v_{dq}^{ref}. To avoid the integrator windup, the voltage integral controller is kept at zero during the current limiting period. Afterward, according to Fig. 1, the current reference i_{fdq}^{ref} can be expressed as

$$i_{fdq}^{ref} = K_P^V(v_{dq}^{ref} - v_{dq}) + i_{dq} + \text{j}\omega_g C_f v_{dq} \tag{2}$$

where K_P^V is the voltage control proportional gain. Notice that $i_{fdq} = i_{dq} + \text{j}\omega_g C_f v_{dq}$ since the dynamics of the capacitor is ignored. Further, with $i_{fdq} = \bar{i}_{fdq}^{ref}$ and (1), (2) is rewritten as

$$i_{fdq} = \sigma K_P^V(v_{dq}^{ref} - v_{dq}) + \sigma i_{fdq} \Rightarrow R_e i_{fdq} = v_{dq}^{ref} - v_{dq} \tag{3}$$

where $R_e \triangleq \frac{1-\sigma}{\sigma K_P^V}$ is a positive real variable.

When the circular current limiter is not triggered, i.e., $\sigma = 1$, then one has $v_{dq} = v_{dq}^{ref}$, which can also be represented by (3) with $R_e = 0$. Therefore, the inner control loop with the circular current limiter can be represented as a voltage source behind equivalent resistance R_e as shown in Fig. 2.

IV. Application for Transient Stability Analysis

A. Closed-Loop System Dynamics

In this section, the closed-loop system dynamics is derived to allow for the transient stability analysis of the converter. Define δ as the angle between the d-axis and v_{gdq}, whose dynamics can be expressed as

$$\dot{\delta} = \omega^{ref} - \omega_g = K_P(P^{ref} - P). \tag{4}$$

In order to derive the closed-loop system dynamics, it requires the relationship between P and δ. Since the capacitor is used to filter out the high-frequency component of the converter-side current, it has a limited impact on transient stability and is hence ignored [4]. The capacitor voltage reference is aligned with the d-axis, i.e., $v_{dq}^{ref} = V^{ref}\text{e}^{\text{j}0}$ with V^{ref} being the voltage reference magnitude. Based on the Kirchhoff circuit law of the equivalent circuit in Fig. 2 and the given voltage sources $v_{dq}^{ref} = V^{ref}$ and $v_{gdq} = V_g\text{e}^{-\text{j}\delta}$ with V_g being the grid voltage magnitude, P can be expressed as a nonlinear function of δ

$$\begin{aligned} P = &\frac{3}{2}\left[\frac{(R_e+R_g)((V^{ref})^2 - V^{ref}V_g\cos\delta)}{(R_e+R_g)^2+\omega_g^2L_g^2} - R_eI_M^2\right. \\ &\left.+\frac{\omega_g L_g V^{ref} V_g \sin\delta}{(R_e+R_g)^2+\omega_g^2L_g^2}\right] \end{aligned} \tag{5}$$

where $R_e = \max\{0, \text{Re}\{\bar{R}_e\}\}$ with

$$\bar{R}_e = \sqrt{\frac{(V^{ref})^2 - 2V^{ref}V_g\cos\delta + V_g^2}{I_M^2} - \omega_g^2L_g^2} - R_g \tag{6}$$

being a state-dependent function. Therefore, the first-order closed-loop system dynamics can be represented by (4) and (5).

B. Transient Stability Analysis

The stability of the first-order nonlinear system in (4) and (5) can be evaluated similarly to the analysis in [9], which is ensured if and only if there exist SEPs.

Two examples of grid voltage drops are given to better illustrate the transient stability of the system. Based on the parameters listed in Table I, the $P-\delta$ curves with $V_g = 1$ p.u. and $V_g = 0.5$ p.u. can be calculated based on (4) and (5). As shown in Fig. 3, when $V_g = 1$ p.u., there are two intersection points between the $P-\delta$ curve and the active power reference P^{ref} for $\delta \in [0, 2\pi)$, where the solid green dot denotes the SEP and the hollow one denotes the unstable equilibrium point (UEP). For $V_g = 0.5$ p.u., no SEP or UEP exists. The green lines demonstrate the theoretically calculated trajectories of the active power outputs under two different conditions.

The first example is shown in the left picture in Fig. 3 with a relatively short period of the grid voltage drop, i.e., the angle δ is smaller than the UEP when the fault is clear. At the beginning, the system is working normally at the SEP. Then the grid voltage drops from 1 p.u. to 0.5 p.u. and the active power output P jumps from the purple line to the pink one. Since $P < P^{ref}$, the angle δ increases according to (4). Afterward, the grid voltage restores to 1 p.u. and P jumps back to the purple line. From the zoomed picture, one can observe that δ is smaller than the UEP and $P > P^{ref}$ after the disturbance. Thus, δ keeps decreasing until it returns to its original operating point.

The second example is shown in the right picture in Fig. 3. Compared with the previous example, the grid voltage drops

This article has been accepted for publication in IEEE Transactions on Power Systems. This is the author's version which has not been fully edited and content may change prior to final publication. Citation information: DOI 10.1109/TPWRS.2022.3173160

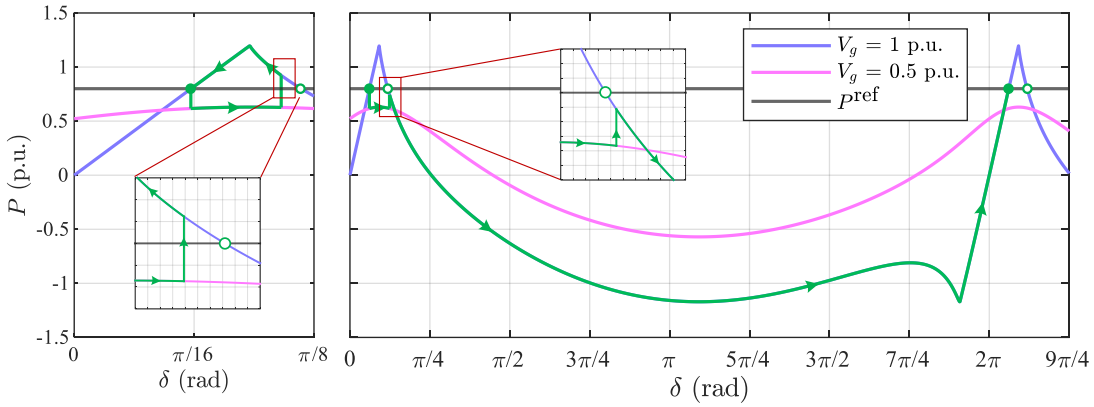

Fig. 3. Examples of transient stability analysis when grid voltage drops from 1 p.u. to 0.5 p.u. (SEP–Solid dot; UEP–Hollow dot).

TABLE I
SYSTEM AND CONTROL PARAMETERS

Quantity	Value
Grid phase voltage V_g	155.56 V (1 p.u.)
Grid angular frequency ω_g	100π rad/s (1 p.u.)
Grid impedance L_g, R_g	11 mH (0.24 p.u.), 0.3 Ω (0.021 p.u.)
LC-filter L_f and C_f	1.5 mH (0.032 p.u.), 15 μF (0.068 p.u.)
Active power reference P^{ref}	2 kW (0.8 p.u.)
Voltage reference V^{ref}	1 p.u.
Power control gain K_P	0.01 p.u.
Maximum current I_M	1.2 p.u.
Voltage control P & I gain	1 p.u., 5 p.u.
Current control P & I gain	1 p.u., 10 p.u.
Switching frequency	10 kHz
Sampling frequency	10 kHz

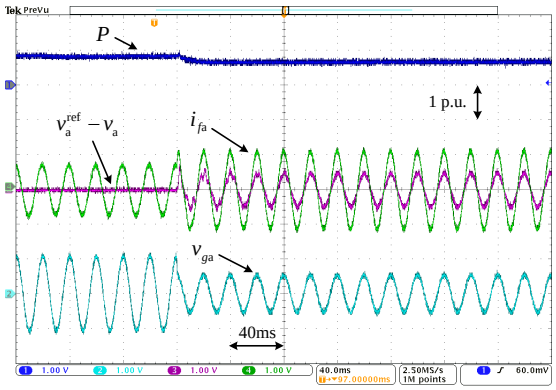

Fig. 4. Experimental results when the grid voltage drops to 0.5 p.u.

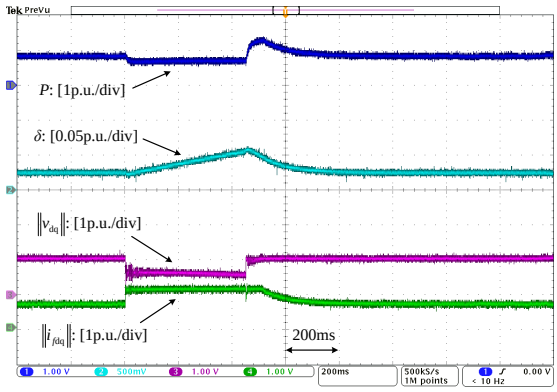

Fig. 5. Experimental results when the grid voltage drops from 1 p.u. to 0.5 p.u. for 450 ms.

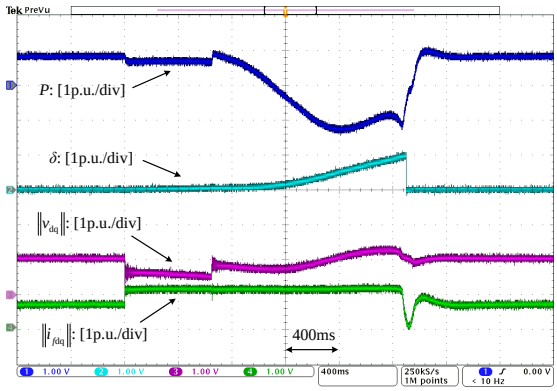

Fig. 6. Experimental results when the grid voltage drops from 1 p.u. to 0.5 p.u. for 650 ms.

for a longer time, and the angle δ is larger than the UEP when the fault is clear. Consequently, when the grid voltage restores to 1 p.u., δ is larger than the UEP and $P < P^{\text{ref}}$ from the zoomed picture. Hence, δ keeps increasing along with the purple line until it stabilizes at the new SEP.

V. EXPERIMENTAL TESTS

The detailed experimental setup can be found in [10] with the system and control parameters listed in Table I. The experimental results are delivered in Figs. 4-6.

The evaluation results of the proposed equivalent circuit model are illustrated in Fig. 4. One can notice that during the pre-fault period, the capacitor voltage can track its reference accurately since the circular current limiter is not triggered. The active power output is kept at its reference value of 0.8 p.u. Afterward, the grid voltage drops to 0.5 p.u. The converter-side current reaches its maximum allowable magnitude of 1.2 p.u., which triggers the circular current limiter. Hence, the capacitor voltage cannot track its reference accurately. During the failure process, the voltage difference $v_{\text{a}}^{\text{ref}} - v_{\text{a}}$ has the same phase as the converter-side current $i_{f\text{a}}$, which means that an equivalent resistor is introduced between the capacitor voltage and its reference to limit the converter-side current. Therefore, the equivalent circuit model developed in Section III is valid.

Fig. 5 presents the results when the grid voltage drops from 1 p.u. to 0.5 p.u. for 450 ms. During the fault period, the converter-side current magnitude is restricted by 1.2 p.u. When

the fault is clear, although the circular current limiter is still triggered for about 50 ms, the active power output, the angle δ, and the capacitor voltage can finally return to their normal operating points.

As shown in Fig. 6, the fault time is increased to 650 ms. Again, the converter-side current magnitude is well restricted. As illustrated in Section IV, since the fault time becomes longer, the angel δ keeps increasing until it stabilizes at a new SEP. Although transient stability is ensured, large fluctuations are observed in the active and reactive power outputs.

VI. Conclusion

This letter reveals the physical insights into the control loops of a GFM converter using a circular current limiter. It is found that the inner control loop with the circular current limiter can be represented by a voltage source behind an equivalent resistor. Based on the developed model, transient stability with the $P - f$ droop control is further investigated. The results reveal that the GFM converter can synchronize with the power grid as long as there exist SEPs. Finally, experimental tests are performed to verify the theoretical analysis. Further studies including applications of the proposed model for the transient stability analysis of multiple GFM converters will be investigated.

References

[1] R. Rosso, X. Wang, M. Liserre, X. Lu, and S. Engelken, "Grid-forming converters: Control approaches, grid-synchronization, and future trends-a review," *IEEE Open J. Ind. Appl.*, vol. 2, pp. 93–109, 2021.

[2] T. Qoria, F. Gruson, F. Colas, X. Kestelyn, and X. Guillaud, "Current limiting algorithms and transient stability analysis of grid-forming VSCs," *Elect. Power Syst. Res.*, vol. 189, p. 106726, 2020.

[3] T. Qoria, F. Gruson, F. Colas, G. Denis, T. Prevost, and X. Guillaud, "Critical clearing time determination and enhancement of grid-forming converters embedding virtual impedance as current limitation algorithm," *IEEE J. Emerg. Sel. Topics Power Electron.*, vol. 8, no. 2, pp. 1050–1061, 2020.

[4] L. Huang, H. Xin, Z. Wang, L. Zhang, K. Wu, and J. Hu, "Transient stability analysis and control design of droop-controlled voltage source converters considering current limitation," *IEEE Trans. Smart Grid*, vol. 10, no. 1, pp. 578–591, 2019.

[5] X. Wang, M. G. Taul, H. Wu, Y. Liao, F. Blaabjerg, and L. Harnefors, "Grid-synchronization stability of converter-based resources–an overview," *IEEE Open J. Ind. Appl.*, vol. 1, pp. 115–134, 2020.

[6] M. G. Taul, X. Wang, P. Davari, and F. Blaabjerg, "Current limiting control with enhanced dynamics of grid-forming converters during fault conditions," *IEEE J. Emerg. Sel. Topics Power Electron.*, vol. 8, no. 2, pp. 1062–1073, 2020.

[7] M. Awal and I. Husain, "Transient stability assessment for current constrained and unconstrained fault ride-through in virtual oscillator controlled converters," *IEEE J. Emerg. Sel. Topics Power Electron.*, vol. 9, no. 6, pp. 6935–6946, 2021.

[8] L. Harnefors, M. Bongiorno, and S. Lundberg, "Input-admittance calculation and shaping for controlled voltage-source converters," *IEEE Trans. Ind. Electron.*, vol. 54, no. 6, pp. 3323–3334, 2007.

[9] H. Wu and X. Wang, "Design-oriented transient stability analysis of grid-connected converters with power synchronization control," *IEEE Trans. Ind. Electron.*, vol. 66, no. 8, pp. 6473–6482, 2019.

[10] B. Fan and X. Wang, "A Lyapunov-based nonlinear power control algorithm for grid-connected VSCs," *IEEE Trans. Ind. Electron.*, vol. 69, no. 3, pp. 2916–2926, 2022.